Ultrathin Films and Hollow Shells with Pillared Architectures Fabricated via Layer-by-Layer Self-Assembly of Titania Nanosheets and Aluminum Keggin Ions

Lianzhou Wang, Yasuo Ebina, Kazunori Takada, and Takayoshi Sasaki*

Advanced Materials Laboratory, National Institute for Materials Science, 1-1 Namiki, Tsukuba, Ibaraki 305-0044, Japan

Received: June 26, 2003; In Final Form: December 5, 2003

Inorganic multilayer films and hollow shells with pillared architectures have been fabricated layer-by-layer on spherical poly(methyl methacrylate) (PMMA) templates as well as flat substrates through the electrostatic self-assembly technique. Positively charged polyoxocations of aluminum Keggin ions were employed both as inorganic binder and as pillaring agent in electrostatic self-assembly with exfoliated unilamellar crystallites of $Ti_{0.91}O_2$, yielding new types of ultrathin films and core−shell composites. Ultraviolet−visible absorption spectra revealed progressive enhancement of absorbance with increasing deposition cycles, indicating the regular growth of multilayer assemblies of titania nanosheets and aluminum polyoxocations. Evolution of a Bragg peak with a periodicity of ca. 1.5 nm and its enhancement also supported the formation of nanostructured multilayer films and shells, accommodating aluminum polyoxocations in the nanosheet gallery. Depth X-ray photoelectron spectra confirmed their inorganic nature. Calcination at 400 °C produced ultrathin films and hollow shells with alumina pillars between the titania sheets. N_2 adsorption results revealed a high specific surface area of 260 m^2 g^{-1} and nanoporous feature for the pillared hollow spheres.

Introduction

There has been considerable interest in the synthesis of layered solids pillared with various inorganic species due to their potential applications as catalyst supports, ion exchangers, molecular sieves, photofunctional materials, etc.[1−3] Pillared materials have been generally synthesized by the intercalation of pillaring agents such as polyoxocations into ionic lamellar hosts and subsequent heat treatment. The recently developed strategy involving exfoliation/restacking processing has opened up a new approach for the design of new pillared materials.[4−7] We have demonstrated that two types of pillared titanates[7] can be obtained by restacking of the nanosheets with aluminum oligometric species $[AlO_4Al_{12}(OH)_{24}(H_2O)_{12}]^{7+}$, known as Al_{13} Keggin ions,[8] as a pillaring agent. The highly positive charge of the clusters effectively induced flocculation of the colloidal titania nanosheets, producing pillared layered titanates. Interestingly, a novel structure with double layers of alumina has been obtained through this route, in addition to the ordinary structure with a single-layer arrangement of pillars. Although pillared materials in bulk form have been widely studied to date, few works have reported the formation of inorganic pillared structures in thin film form[9] or in well-defined morphology.

The recently established electrostatic layer-by-layer (LBL) self-assembly method is one of the most powerful techniques for tailoring nanostructured thin films and has been successfully applied to the structural organization of various charged species, including polyelectrolytes, proteins, dyes, inorganic nanoparticles, and nanosheets.[10−14] This approach provides excellent control over the film thickness and nanoarchitecture, and its versatility and simplicity have opened up new possibilities in both fundamental and applied fields. In addition to the fabrication of thin films on planar substrates, the LBL technique has also been extended to the preparation of nanocoatings on colloidal supports, yielding so-called "core−shell" structures. A number of works have focused on the fabrication of core−shell composites using molecular precursors and nanoparticles as inorganic shell building blocks through the LBL self-assembly procedure.[15−18] We have recently demonstrated the fabrication of core−shell particles by deposition of exfoliated titania nanosheets onto polymer beads.[19] The ultrathin and highly flexible nature of titania nanosheets allowed the shell thickness to be easily controlled stepwise on a nanometer scale. Hollow titania shells with controllable ultrathin thickness were derived via core removal by heating or UV irradiation.

Organic polyelectrolytes have widely been employed as molecular "binders" or "glues" in electrostatic self-assembly to produce inorganic−organic hybrid films and core−shell composites,[20] whereas inorganic binders have attracted much less attention. In comparison with organic glues, inorganic binders may be advantageous in providing novel architectures and new properties for multilayer films, such as better thermal stability and new physicochemical properties due to the contribution of inorganic binders themselves.

This paper describes the fabrication of titania multilayer films and hollow shells with use of polyoxocations of Al_{13} Keggin ions as inorganic binder. Actually, Al_{13} polyoxocations have been employed to modify the substrate surface and multilayer film fabrication.[21] However, the information concerning the architecture of thin films was limited. Furthermore, the technique has not been applied to important materials such as titanium oxides. In the present study, we demonstrate the successful LBL assembly of positively charged Al_{13} clusters and exfoliated titania nanosheets both on planar and on spherical supports, yielding new types of inorganic multilayer films and hollow shells. The obtained films and shells had a pillared structure, resulting in nanoporous nature.

* Address correspondence to this author. E-mail: sasaki.takayoshi@nims.go.jp, Fax: +81-29-854-9061.

10.1021/jp035818w CCC: $27.50
Published on Web 03/16/2004

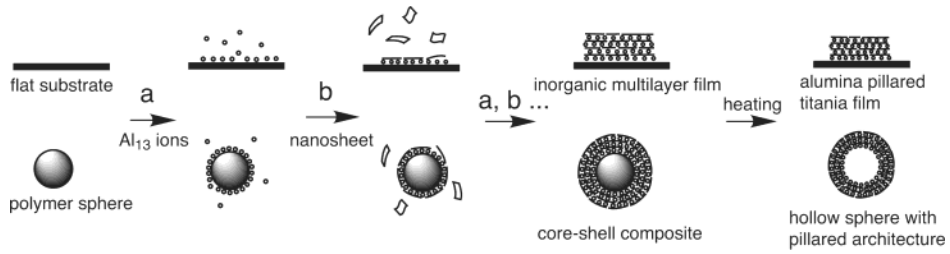

Figure 1. Schematic illustration of the procedures for fabricating inorganic multilayer films and hollow titania shells with a pillared structure. Polymer spheres, Al_{13} polyoxocations, and titania nanosheets are indicated in the figure.

Experimental Section

Materials. Reagents, such as NaOH (Wako Pure Chemical Co.) and $Al(NO_3)_3 \cdot 9H_2O$ (Kanto Chemical Co., Japan), were of analytical grade. Poly(methyl methacrylate) (PMMA) beads with an average diameter of 0.4 μm were purchased from Soken Chemical Co. A colloidal suspension containing exfoliated titania nanosheets, $Ti_{0.91}O_2$, was synthesized according to a previously reported method.[22] Ultrapure water with resistivity of >18 MΩ cm was obtained from a Milli-Q water purification system and used throughout the experiments.

Al_{13} Keggin Ions. A pillaring solution containing Al_{13} Keggin ions was prepared by hydrolyzing an aluminum salt.[7b] In a typical experiment, 300 cm^3 of 0.2 mol dm^{-3} NaOH solution was added dropwise under stirring into 120 cm^3 of 0.2 mol dm^{-3} $Al(NO_3)_3$ solution at a rate of 1 cm^3 min^{-1} at room temperature. The resulting transparent solution was aged overnight before use. The concentration of Al_{13} Keggin ions was ca. 4.4×10^{-3} mol dm^{-3} based on the Al content in the starting $Al(NO_3)_3$ solution.

Self-Assembly of Multilayer Films. The cleaning of solid substrates, such as Si wafers and quartz glass slides, was carried out according to the procedures described previously.[14b] Multilayer films were fabricated by sequential deposition of Al_{13} polyoxocations and titania nanosheets on a substrate. A substrate was immersed first in an aqueous solution containing Al_{13} clusters (concentration, ca. 9×10^{-4} mol dm^{-3}; pH ~5.0) for 20 min. After being washed thoroughly with pure water, the substrate was dipped into the colloidal suspension containing $Ti_{0.91}O_2$ nanosheets (0.08 g dm^{-3}) for 20 min, followed by thorough washing with pure water. Its pH value was carefully adjusted to 7 by adding an appropriate amount of a diluted HCl solution. This procedure was repeated a desired number of times to obtain thin films of $(Al_{13}/Ti_{0.91}O_2)_n$.

Fabrication of Core−Shell Particles and Hollow Shells. In a typical synthetic procedure, 0.5 g of PMMA spherical particles was dispersed in 150 cm^3 of a solution of Al_{13} Keggin ions (concentration, ca. 3×10^{-4} mol dm^{-3}) under stirring. Then the suspension was ultrasonically treated for 10 min to disperse the PMMA particles homogeneously and further stirred for another 15 min to ensure the saturated adsorption of Al_{13} polyoxocations on the PMMA surface. Excess Al_{13} ions were removed by centrifugation (5500 rpm, 5 min) and water washing. The recovered PMMA beads coated with Al_{13} Keggin ions were dispersed in 150 cm^3 of H_2O again and ultrasonically agitated for another 10 min to avoid the possible aggregation of the particles. Then, 5 cm^3 of the colloidal suspension of $Ti_{0.91}O_2$ nanosheets (concentration, 4 g dm^{-3}) was added under stirring. Upon addition of the suspension, some flocculated aggregates were observed, which were formed due to the electrostatic interaction of the negatively charged nanosheets and Al_{13}-primed PMMA surface. Titania nanosheets were used in excess to promote dense coverage of the particle surface. Finally, the sample was recovered by filtration and washing. The above procedure was repeated n cycles to fabricate a core−shell composite coated with alternating multilayers of $(Al_{13}/Ti_{0.91}O_2)_n$.

To obtain hollow spheres, the core−shell particles were heated from room temperature at a rate of 1 °C min^{-1} and held at a desired temperature under oxygen gas flow for 4 h.

Characterizations. The surface topography of the films was examined with a Seiko SPA400 atomic force microscope (AFM) in tapping mode with silicon-tip cantilevers (20 N m^{-1}). Ultraviolet−visible (UV−vis) absorption spectra were collected with a Hitachi U-4000 spectrometer equipped with an integrating sphere detection system. X-ray diffraction (XRD) data were acquired by a Rigaku Rint 2000 powder diffractometer with Cu Kα radiation ($\lambda = 0.15405$ nm). X-ray photoelectron spectra (XPS) were recorded on a Physical Electronics XPS-5700 spectrometer with Al Kα X-ray line (1486.6 eV). A JEOL-1010 transmission electron microscope (TEM) operated at 100 kV was employed to obtain TEM images and electron diffraction patterns. Thermal analysis measurements (TGA) were carried out under airflow on a Rigaku TG-8120 instrument at a heating rate of 1 °C min^{-1}. Nitrogen adsorption−desorption isotherms were measured with a BELSORP 28SA instrument. A sample was pretreated by treating at 150 °C under evacuation for 10 h prior to measurements. The specific surface area (S_{BET}) was calculated from a linear part of the BET plot ($P/P_0 = 0.05-0.30$) while the pore size distribution was determined from the adsorption branch of the N_2 isotherm by employing the Dollimore-Heal (DH) method.

Results and Discussion

Figure 1 schematically outlines the fabrication procedures of multilayer ultrathin films and hollow spheres with pillared architectures. The surfaces of flat substrates and spherical polymer templates are coated with Al_{13} Keggin ions and then with titania nanosheets. Repetition of this bilayer deposition leads to multilayer thin films and core−shell nanocomposites. The resulting inorganic multilayer films and core−shell particles are finally calcined to produce porous thin films and hollow spheres with a pillared structure.

LBL Assembly of Multilayer Films. The growth of self-assembled thin films was initiated by coating a flat substrate with Al_{13} Keggin ions, followed by adsorption of colloidal $Ti_{0.91}O_2$ nanosheets. The deposition parameters are essential for the fabrication of multilayer films with a well-defined nanoarchitecture. We selected the deposition conditions for nanosheets as follows: concentration, 0.08 g dm^{-3}; pH 7; and duration time, 20 min, which have been well established in our previous work.[14] In contrast, information on the adsorption of Al_{13} polyoxocations is scarce. We examined how Al_{13} concentration and deposition time influence the multilayer buildup. The multilayer film growth can be monitored by UV−vis spectra, which exhibit a sharp UV absorption band centered at around 260 nm after the deposition step of $Ti_{0.91}O_2$ nanosheets. This

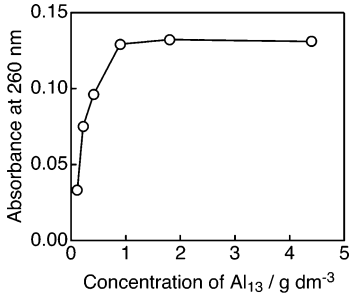

Figure 2. UV−vis absorbance at 260 nm after adsorption of Al_{13}/$Ti_{0.91}O_2$ bilayers as a function of Al_{13} concentration. Nanosheet concentration, 0.08 g dm^{-3}; pH , ∼5.0 for the Al_{13} pillaring solution and 7.0 for the nanosheet suspension; deposition time, 20 min each.

optical absorption is characteristic of delaminated titania nanosheets.[14] On the other hand, Al_{13} Keggin ions gave negligible spectral contribution. Because Al_{13} polyoxocations and $Ti_{0.91}O_2$ nanosheets were alternately deposited, accompanied by charge reversal, the absorbance enhancement at 260 nm provides information on how Al_{13} Keggin ions as well as $Ti_{0.91}O_2$ nanosheets were absorbed. Figure 2 depicts the UV−vis peak-top absorbance after the deposition of the first Al_{13}/$Ti_{0.91}O_2$ bilayer when a solution of Al_{13} Keggin ions with various concentrations was applied (the deposition time was fixed to 20 min). The absorbance of titania increased with increasing the Al_{13} concentration up to 0.9 g dm^{-3}. This may be reasonably explained by the adsorption of a larger amount of Al_{13} Keggin ions at a higher solution concentration, which should provide larger electrostatic attraction force toward the oppositely charged nanosheets. Further increment of the Al_{13} concentration above 0.9 g dm^{-3} did not lead to the enhancement of UV absorbance due to titania nanosheets, implying a similar loading amount of Al_{13} polyoxocations on the substrate surface in this concentration range. The effect of adsorption time was also examined by fixing the Al_{13} concentration of 0.9 g dm^{-3}, which revealed no noticeable enhancement of absorbance with deposition times longer than 20 min. We therefore selected the concentration at 0.9 g dm^{-3} and the duration of 20 min for deposition of Al_{13} polyoxocations. The successful adsorption of Al_{13} polyoxocations onto a bare surface of quartz glass and silicon wafer may be ascribed to the interaction between the highly positive charge of +7 for Al_{13} Keggin ions and surface hydroxyl groups. Similar phenomena have been reported previously.[21]

The pillaring solution of Al_{13} Keggin ions was stable at a pH value of ∼5.0.[7] In contrast, the colloidal $Ti_{0.91}O_2$ nanosheets were well dispersed under the basic condition (pH >7). The suspension tended to undergo partial flocculation in a pH range of 5−6 and produce an aggregated precipitate at a lower pH value. This contradictory behavior should be resolved in the film fabrication. In the multilayer buildup, we fixed the pH value of the Al_{13} solution at 5 and adjusted the titania nanosheet suspension to pH 7 using an appropriate amount of a diluted HCl.

The AFM image shown in Figure 3 visualizes the surface topography of the first deposited layer of $Ti_{0.91}O_2$ nanosheets on top of the Al_{13}-coated Si wafer. Al_{13} polyoxocations themselves were not perceptible. The substrate surface was densely covered with titania nanosheets with a lateral size distribution ranging from hundreds of nanometers to 1 μm. The coverage was similar to that for ultrathin films fabricated with $Ti_{0.91}O_2$ nanosheets and organic polyelectrolytes;[14b] the monolayer deposition was predominant while there were some uncovered areas and overlapped patches. The overall coverage was determined to be about 89% and the overlapped percentage

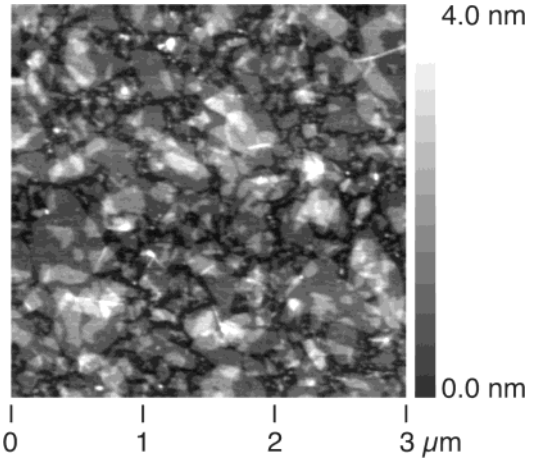

Figure 3. Tapping-mode AFM image of the first titania nanosheet layer on an Si wafer precoated with Al_{13} polyoxocations. Nanosheet concentration, 0.08 g dm^{-3}; pH of nanosheet suspension, 7.

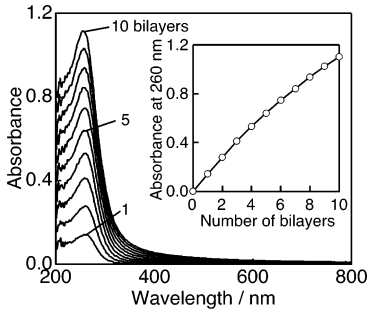

Figure 4. UV−vis absorption spectra of the $(Al_{13}/Ti_{0.91}O_2)_n$ multilayer film fabricated on a quartz glass substrate. Nanosheet concentration, 0.08 g dm^{-3}; deposition time, 20 min; pH 7. The insert shows the dependence of absorbance at 260 nm as a function of deposition cycle.

was ca. 30%. This indicates that inorganic Al_{13} clusters can play a comparable role to that for the widely used organic polymer.

The progressive growth of $Al_{13}/Ti_{0.91}O_2$ multilayer films under the optimized conditions was examined by UV−vis adsorption (Figure 4) measured immediately after each deposition cycle. The nearly linear increment of peak-top absorbance at 260 nm indicates that an approximately equal amount of $Ti_{0.91}O_2$ nanosheets was deposited in each cycle, clearly demonstrating the successful LBL assembly of multilayer ultrathin films with use of Al_{13} polyoxocations as inorganic binder. The absorbance of ca. 1.1 after deposition of 10 bilayers was similar to that observed for a comparable multilayer assembly with polyelectrolytes.[14]

Characterizations of the Films. XRD patterns for the multilayer thin films of $(Al_{13}/Ti_{0.91}O_2)_n$ revealed the evolution of diffraction peaks indicating a spacing of ca. 1.5 nm (see Figure 5). With increasing numbers of bilayers, their intensity enhanced. In addition, the second-order peaks became better resolved. These diffraction features are attributable to the repeating bilayers of $Al_{13}/Ti_{0.91}O_2$**.** The crystallographic thickness of $Ti_{0.91}O_2$ nanosheets is 0.7 nm,[22] and the diameter of the Al_{13} cluster is 0.86 nm when approximated as a spherical body.[3b] Accordingly, the expected repeating distance of the $Al_{13}/Ti_{0.91}O_2$ bilayer should be 1.5−1.6 nm, which agrees well with the experimental value. Similar basal distance has been reported for layered titanates with pillars of Al_{13} polyoxocations synthesized in bulk.[7b,23]

XPS survey scan for the film of $(Al_{13}/Ti_{0.91}O_2)_{10}$ detected signals from C, O, Ti, and Al. Figure 6a shows signals from Ti (2p) core levels, at 459.3 and 465.1 eV for Ti ($2p_{3/2}$) and Ti

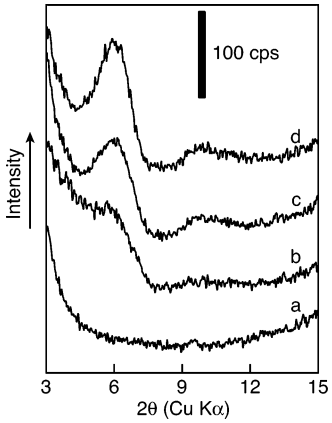

Figure 5. XRD pattern of as-prepared multilayer thin films of $(Al_{13}/Ti_{0.91}O_2)_n$: n is = 1 (a), 3 (b), 5 (c), and 10 (d).

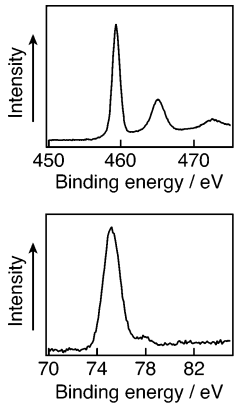

Figure 6. High-resolution XPS spectra in the (a) Ti 2p and (b) Al 2p regions for the $(Al_{13}/Ti_{0.91}O_2)_{10}$ thin film.

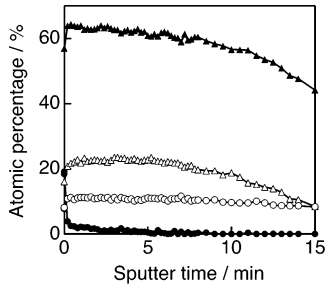

Figure 7. Atomic percentage of a film of $(Al_{13}/Ti_{0.91}O_2)_{10}$ as a function of sputter time in depth XPS analysis. The symbols of filled triangles, open triangles, filled circles, and open circles represent the signals from O, Ti, C, and Al, respectively.

($2p_{1/2}$) lines,[24] respectively, which are assignable to $Ti_{0.91}O_2$ nanosheets. The Al (2p) peak was detected at a binding energy of 75.2 eV (Figure 6b), which is direct evidence for the incorporation of Al_{13} polyoxocations in the film. Carbon was found to be present at the very surface by XPS depth analysis using an Ar^+ gun (Figure 7). This strongly suggests that the C signal is attributable to hydrocarbons adsorbed from ambient atmosphere as contamination, as is frequently observed in other thin films.[14c,25] The C content drastically dropped to a negligible level (<1%) by sputtering for a short time, confirming the inorganic nature of the multilayer film. A relatively steady state was reached at the etching time of 2−5 min, where the contents of Ti, Al, and O should more reliably reflect the chemical composition of the film. The average atomic ratio of Ti to Al in the film was 2.1.

It is of interest to discuss the nanoarchitecture of the resulting multilayer film. As reported previously,[14b] the two-dimensional

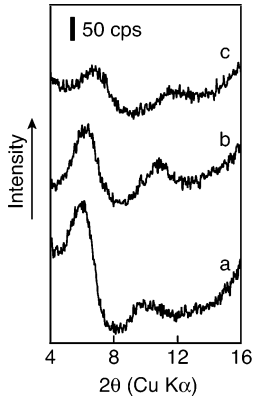

Figure 8. XRD patterns of the thin film of $(Al_{13}/Ti_{0.91}O_2)_{10}$ heated at different temperatures: (a) 100 °C × 1 h; (b) 200 °C × 1 h; and (c) 400 °C × 1 h. The slant baseline arises from an amorphous hump from a quartz substrate.

unit cell area of titania nanosheets is 0.114 nm^2 (=0.38 nm × 0.30 nm), containing two units of $Ti_{0.91}O_2$ with a net negative charge of 0.70^-. On the other hand, the Al_{13} polyoxocation, $[AlO_4Al_{12}(OH)_{24}(H_2O)_{12}]^{7+}$, is approximately spherical in shape with a diameter of 0.86 nm.[3b] Its volume is 0.333 nm^3. From the viewpoint of electrostatic balance, 10 unit cells of the titania nanosheet should be necessary to compensate for the positive charge of one Al_{13} Keggin ion. Accordingly, the calculated atomic ratio of Ti to Al in the film should be 1.4 (=10 × 0.91 × 2/13), which is smaller than that determined by XPS (2.1). Taking the surface coverage of titania nanosheets (~120% determined by AFM image in Figure 3) into account, the calculated value of 1.7 may be compatible with that from the experimental data.

The net clearance space in the multilayer assembly has a height of 0.80 nm by subtracting the nanosheet thickness of 0.70 nm from the multilayer repeating distance of 1.5 nm. Consequently, the space occupied by Al_{13} Keggin ions in the nanosheet gallery is estimated to be ~37% (0.333 nm^3/(0.114 nm^2 × 10 × 0.8 nm)). The estimation suggests the sparse distribution of Al_{13} clusters although it is based on an approximate structural consideration. This structural feature gives this multilayer system its porous nature.

The multilayer film of $(Al_{13}/Ti_{0.91}O_2)_{10}$ was heated at different temperatures to examine the structural stability (Figure 8). The characteristic diffraction peak of $d \approx 1.5$ nm remained almost unchanged at 100 °C. Heating at higher temperatures resulted in a gradual internanosheet contraction, which may be attributable to the shrinkage of aluminum oligometric species of $[AlO_4Al_{12}(OH)_{24}(H_2O)_{12}]^{7+}$ due to dehydroxylation upon heating.[26] The basal spacing was ca. 1.3 nm upon heating at 400 °C, suggesting that the pillared structure survived. Similar XRD results have been obtained in various pillared materials synthesized in bulk form.[7] The interlayer spacings shrank continuously at higher temperatures and then disappeared above 600 °C, indicating the collapse of the multilayer structure.

Hollow Shells with a Pillared Structure. The alternate electrostatic adsorption of Al_{13} clusters and titania nanosheets on PMMA beads produced core−shell composites. XRD data of the PMMA shells provided the evidence for the formation of shell structures on the polymer templates (see Figure 9). The bare PMMA exhibited two humps centered at $2\theta = 14.0°$ and 30.5°. These halo patterns were suppressed significantly upon shell assembly, suggesting the coverage of PMMA cores with shell materials. A diffraction peak centered at $2\theta = 5.8°$ appeared after several coating cycles. Its spacing of ca. 1.5 nm

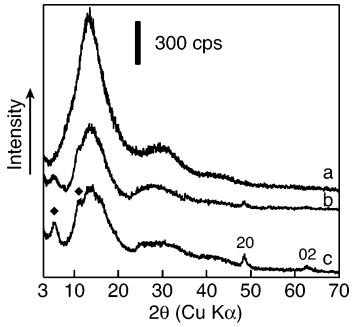

Figure 9. XRD patterns of core−shell nanocomposites: (a) bare PMMA spheres and (b, c) PMMA spheres coated with 5 and 10 bilayers of $Al_{13}/Ti_{0.91}O_2$, respectively. Diamonds indicate the Bragg peak with a basal spacing of ca. 1.5 nm. All the data were collected with a similar amount of sample.

coincides with that for multilayer films on a flat substrate, again being attributable to the repeated layer pairs of $Al_{13}/Ti_{0.91}O_2$. A progressive enhancement in peak intensity with increasing cycles was observed, indicating the growth of a nanostructured shell of Al_{13} polyoxocations and $Ti_{0.91}O_2$ nanosheets on PMMA surfaces. The additional peaks at around $2\theta = 48.1°$ and 62.6° were clearly identified for a film with a larger number of bilayers. These peaks are assignable to 20 and 02 diffraction bands arising from a two-dimensional atomic arrangement (0.38 nm × 0.30 nm) in the nanosheets.[19]

The heating process of the core−shell composites was followed by thermal analysis measurements. A huge weight loss was observed between 250 and 350 °C, accompanied by a pronounced exothermic peak. The combustion of PMMA cores is responsible for this thermal event. No apparent weight loss occurred above 400 °C. Consequently, the core−shell composites were heated at 400 °C to remove the polymer cores. TEM observations for the calcined product with 10 bilayers of $Al_{13}/Ti_{0.91}O_2$ visualized spherical hollow shells, confirming the successful removal of PMMA (Figure 10a). The spherical shape of the polymer beads as templates was preserved, which is comparable with those titania hollow shells prepared with organic binder.[19] The average diameter of hollow shells was in a range of 360−380 nm, indicating 5−10% shrinkage in comparison with that for original PMMA templates. High-magnification TEM images revealed that the shell thickness was around 10−15 nm (Figure 10b). This is reasonable for a dimension of 10 bilayers of $(Al_{13}/Ti_{0.91}O_2)$. The electron diffraction pattern of shells (Figure 10c) was composed of a series of diffraction rings. The indices and spacings for rings 1−4 are 10 (0.371 nm), 20 (0.192 nm), 02 (0.154 nm), and 22 (0.121 nm), respectively,[27] for the two-dimensional unit cell (0.38 nm × 0.30 nm) of the nanosheet structure, providing evidence for the intactness of nanosheets upon heat treatment at 400 °C.

Figure 11 presents the XRD pattern of hollow shells. Basal diffraction peaks showing a spacing of ca. 1.4 nm were present. In addition, 20 and 02 diffraction bands reflecting the intrananosheet structure were observed. These diffraction features are compatible with the pillared structure. Similar XRD results have been obtained for multilayer films above and also for pillared titanates synthesized in bulk.[7b] This suggests the formation of pillared architecture in alumina pillared titania hollow shells. The hollow titania shells, derived by heating the core−shell particles with a nanosheet/polyelectrolyte shell, were composed of anatase.[19] Crystallization of anatase from titania nanosheets in this material was promoted upon the removal of polymers from nanosheet galleries. In contrast, Al_{13} polyoxocations as inorganic binders play a role as pillars, isolating the nanosheets and suppressing the anatase crystallization.

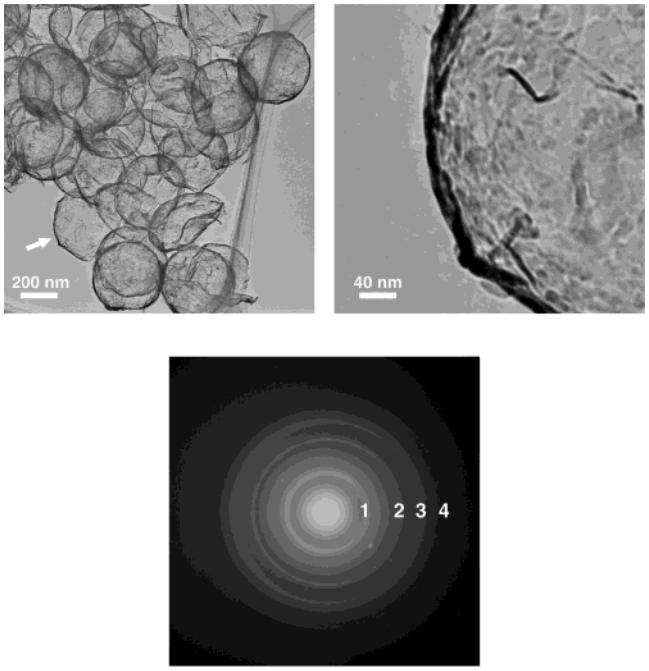

Figure 10. TEM images of (a) hollow spheres obtained by the calcination of core−shell composite with a shell of $(Al_{13}/Ti_{0.91}O_2)_{10}$ at 400 °C; (b) high-magnification image showing the wall thickness (area marked by arrow in part a); and (c) electron diffraction pattern of hollow shells.

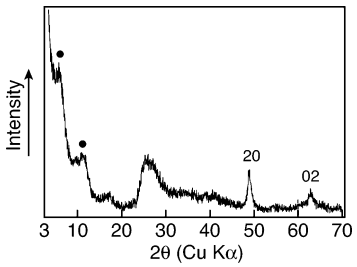

Figure 11. XRD pattern of alumina pillared titania hollow spheres prepared by calcination at 400 °C. Circles indicate the basal peaks for the pillaring structure.

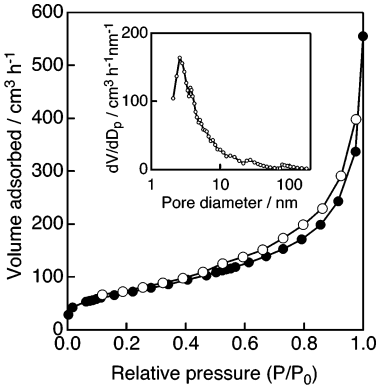

Figure 12. Nitrogen adsorption−desorption isotherms and pore size distribution of alumina pillared titania hollow shells (inset).

Figure 12 shows the nitrogen adsorption−desorption isotherms of the hollow shells, which can be classified as type IV, characteristic of mesoporous materials.[28] The observed hysteresis loop between adsorption and desorption branches can be considered as type H3, the feature of slitlike pores. Similar N_2 adsorption behaviors have been reported for pillared titanates.[7]

Pore size distribution analysis revealed that the average pore diameter was around 3 nm, accompanying small portions of larger pores. The specific surface area determined by the multipoint Brunauer−Emmett−Teller (BET) method was about 260 $m^2\ g^{-1}$, which is larger than that (∼160 $m^2\ g^{-1}$) for a comparable pillared titanate synthesized in bulk.[7] T-plot analysis indicated the presence of both micropores and mesopores in the materials with a microporous surface area of ca. 73 $m^2\ g^{-1}$. The anatase hollow shells mentioned above[19] had a surface area value of ca. 140 $m^2\ g^{-1}$. These data evidently indicate that incorporation of Al_{13} polyoxocations contributes to the enhancement of surface area via the porous structure formation in the shell. The hollow shells (360−380 nm in diameter) with micro/mesoporous walls are characterized by a hierarchical structure containing a series of nanoporosities. Thus, this may be regarded as a new class of porous materials.

In summary, we have demonstrated the successful fabrication of inorganic multilayer ultrathin films and hollow spheres via self-assembly of titania nanosheets and Al_{13} Keggin ions. The characterizations revealed the well-defined pillared structure. The hollow shells may be catalogued as a new type of porous materials, possessing a hierarchical nanoporous architecture. The modification and encapsulation of these pillared systems with functional species such as noble metals and dyes are now underway, and may find applications in photoelectric conversion and photocatalysis.

Acknowledgment. This work was supported by CREST, Japan Science and Technology Agency (JST).

References and Notes

(1) (a) Pinnavaia, T. J. *Science* **1983**, *220*, 365. (b) Clearfield, A. *Chem. Rev.* **1988**, *88*, 125.

(2) Mallouk, T. E.; Gavin, J. A. *Acc. Chem. Res.* **1998**, *31*, 209.

(3) (a) Ogawa, M.; Kuroda, K. *Chem. Rev.* **1995**, *95*, 399. (b) Ohtsuka, K. *Chem. Mater.* **1997**, *9*, 2030.

(4) (a) Domen, K.; Ebina, Y.; Ikeda, S.; Tanaka, A.; Kondo, J. N.; Maruya, K. *Catal. Today* **1996**, *28*, 167. (b) Ebina, Y.; Sasaki, T.; Harada, M.; Watanabe, M. *Chem. Mater.* **2002**, *14*, 4390.

(5) (a) Xu, Y.-H.; Feng, Q.; Kajiyoshi, K.; Yanagisawa, K.; Yang, X.-J.; Makita, S.; Ooi, K. *Chem. Mater.* **2002**, *14*, 3844. (b) Liu, Z.-H.; Yang, X.-J.; Makita, Y.; Ooi, K. *Chem. Mater.* **2002**, *14*, 4800.

(6) Liu, P.; Gong, K.; Xiao, P.; Xiao, M. *J. Mater. Chem.* **2000**, *10*, 933.

(7) (a) Kooli, F.; Sasaki, T.; Watanabe, M. *Chem. Commun.* **1999**, 211. (b) Kooli, F.; Sasaki, T.; Watanabe, M. *Microporous Mesoporous Mater.* **1999**, *28*, 495. (c) Kooli, F.; Sasaki, T.; Rives, V.; Watanabe, M. *J. Mater. Chem.* **2000**, *10*, 497. (d) Kooli, F.; Sasaki, T.; Watanabe, M. *Langmuir* **1999**, *15*, 1090.

(8) (a) Keggin, J. F. *Nature* **1933**, *131*, 908. (b) Fu, G.; Nazar, L. F.; Bain, A. D. *Chem. Mater.* **1991**, *3*, 602.

(9) Sumida, T.; Abe, R.; Hara, M.; Kondo, J. N.; Domen, K. *J. Mater. Res.* **2000**, *15*, 2587.

(10) (a) Decher, G. *Science* **1997**, *277*, 1232. (b) Fendler, J. H. *Chem. Mater.* **1996**, *8*, 1616. (c) Cassagneau, T.; Fendler, J. H.; Mallouk, T. E. *J. Am. Chem. Soc.* **1998**, *120*, 7848.

(11) (a) Caruso, F.; Möhwald, H. *J. Am. Chem. Soc.* **1999**, *121*, 6039. (b) Lvov, Y.; Ariga, K.; Ichinose, I.; Kunitake, T. *J. Am. Chem. Soc.* **1995**, *117*, 6117. (c) Fang, M.-M.; Kaschak, D. M.; Sutorik, A. C.; Mallouk, T. E. *J. Am. Chem. Soc.* **1997**, *119*, 12184.

(12) (a) Rogach, A. L.; Koktysh, D. S.; Harrison, M.; Kotov, N. A. *Chem. Mater.* **2000**, *12*, 1526. (b) Gao, M. Y.; Richter, B.; Kirstein, S.; Möhwald, H. *J. Phys. Chem. B* **1998**, *102*, 4096.

(13) (a) Schrof, W.; Rozouvan, S.; Keuren, E. V.; Horn, D.; Schmitt, J.; Decher, G. *Adv. Mater.* **1998**, *10*, 338. (b) Ostrander, J. W.; Mamedov, A. A.; Kotov, N. A. *J. Am. Chem. Soc.* **2001**, *123*, 1101.

(14) (a) Sasaki, T.; Ebina, Y.; Watanabe, M.; Decher, G. *Chem. Commun.* **2000**, 2163. (b) Sasaki, T.; Ebina, Y.; Tanaka, T.; Harada, M.; Watanabe, M.; Decher, G. *Chem. Mater.* **2001**, *13*, 4661. (c) Sasaki, T.; Ebina, Y.; Fukuda, K.; Tanaka, T.; Harada, M.; Watanabe, M. *Chem. Mater.* **2002**, *14*, 3524.

(15) (a) Caruso, F.; Caruso, R. A.; Möhwald, H. *Science* **1998**, *282*, 1111. (b) Davies, R.; Schurr, G. A.; Meenan, P.; Nelson, R. D.; Bergna, H. E.; Brevett, C. A. S.; Goldbaum, R. H. *Adv. Mater.* **1998**, *10*, 1264.

(16) (a) Caruso, F. *Adv. Mater.* **2001**, *13*, 11. (b) Caruso, R. A.; Susha, A.; Caruso, F. *Chem. Mater.* **2001**, *13*, 400. (c) Rogach, A.; Susha, A. S.; Caruso, F.; Sukhorukov, G.; Kornowski, A.; Kershaw, S.; Möhwald, H.; Eychmüller, A.; Weller, H. *Adv. Mater.* **2000**, *12*, 333.

(17) (a) Keller, S. W.; Johnson, S. A.; Brigham, E. S.; Yonemoto, E. H.; Mallouk, T. E. *J. Am. Chem. Soc.* **1995**, *117*, 12879. (b) Chen, T.; Somasundaran, P. *J. Am. Ceram. Soc.* **1998**, *81*, 140.

(18) (a) Guo, X.-C.; Dong, P. *Langmuir* **1999**, *15*, 5535. (b) Giersig, M.; Ung, T.; Liz-Marzan, L. M.; Mulvaney, P. *Adv. Mater.* **1997**, *9*, 570.

(19) Wang, L. Z.; Sasaki, T.; Ebina, Y.; Kurashima, K.; Watanabe, M. *Chem. Mater.* **2002**, *14*, 4827.

(20) Tripathy, S. K.; Kumar, J.; Nalwa, H. S. *Handbook of Polyelectrolytes and Their Applications*; American Scientific Publishers: Los Angeles, CA, 2002.

(21) (a) Ollivier, P. J.; Kovtyukhova, N. I.; Keller, S. W.; Mallouk, T. E. *Chem. Commun.* **1998**, 1563. (b) Keller, S. W.; Kim, H. N.; Mallouk, T. E. *J. Am. Chem. Soc.* **1994**, *116*, 8817.

(22) (a) Sasaki, T.; Watanabe, M.; Hashizume, H.; Yamada, H.; Nakazawa, H. *J. Am. Chem. Soc.* **1996**, *118*, 8329. (b) Sasaki, T.; Watanabe, M. *J. Am. Chem. Soc.* **1998**, *120*, 4682.

(23) (a) Anderson, M. W.; Klinowski, J. *Inorg. Chem.* **1990**, *29*, 3260. (b) Hou, W.; Yan, Q.; Peng, B.; Fu, X. *J. Mater. Chem.* **1995**, *5*, 109. (c) Cheng, S.; Wang, T. *Inorg. Chem.* **1989**, *28*, 1283.

(24) Moulder, J.; Stickle, W.; Sobol, P.; Bomben, K. *Handbook of X-ray Photoelectron Spectroscopy*; Chastain, J., Ed.; Perkin-Elmer Corp.: Eden Prairie, MN, 1992.

(25) (a) Wang, Z.-S.; Sasaki, T.; Muramatsu, M.; Ebina, Y.; Tanaka, T.; Wang, L. Z.; Watanabe, M. *Chem. Mater.* **2003**, *15*, 807. (b) Wang, L. Z.; Omomo, Y.; Sakai, N.; Fukuda, K.; Nakai, I.; Ebina, Y.; Takada, K.; Watanabe, M.; Sasaki, T. *Chem. Mater.* **2003**, *15*, 2873.

(26) Galván, J. C.; Jiménez-Morales, A.; Jiménez, R.; Merino, J.; Villanueva, A.; Crespin, M.; Aranda, P.; Ruiz-Hitzky, E. *Chem. Mater.* **1998**, *10*, 3379.

(27) Sasaki, T.; Ebina, Y.; Kitami, Y.; Watanabe, M.; Oikawa, T. *J. Phys. Chem. B* **2001**, *105*, 6116.

(28) Sing, K. S. W.; Everett, D. H.; Haul, R. A. W.; Moscou, L.; Pireotti, R. A.; Rouquérol, J.; Siemieniewska, T. *Pure. Appl. Chem.* **1985**, *57*, 603.